

# High-resolution structural analysis of the cyanobacterial photosystem I complex reveals independent incorporation of small transmembrane and cytoplasmic subunits

Dear Editor,

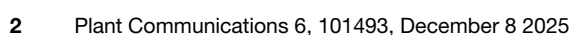
Photosynthetic energy conversion, essential for life on Earth, is performed by cyanobacteria, algae, and plants using photosystem I (PSI) and II (PSII). These membrane complexes consist of numerous protein subunits and cofactors, including chlorophylls (Chls), carotenoids, quinones, and lipids. They transfer electrons from water to  $\text{NADP}^{+}$ , which is then used for  $\text{CO}_2$  fixation together with ATP. The PSI core consists of the large transmembrane (TM) subunits PsaA and PsaB (Caspary et al., 2020), which hold cofactors required for electron transfer, including special Chls, quinones, and the  $[4\text{Fe-4S}]$  cluster  $F_X$ . Cytoplasmic PsaC, stabilized by its neighboring PsaD and PsaE subunits, binds two additional  $[4\text{Fe-4S}]$  clusters,  $F_A$  and  $F_B$ , which accept electrons from  $F_X$  and reduce ferredoxin or flavodoxin, driving downstream metabolic processes (Caspary et al., 2020; Kanda et al., 2021). Smaller TM subunits, including PsaF, PsaI, PsaJ, PsaK, PsaL, and PsaM, are also important for the optimal function and structure of PSI (Malavath et al., 2018; Caspary et al., 2020). PSI typically forms trimers in cyanobacteria (Malavath et al., 2018) but exists as monomers or dimers in algae (Naschberger et al., 2022) and plants (Caspary et al., 2020). Although the structure of mature PSI has been extensively characterized, its assembly in photosynthetic cells remains to be fully clarified. PSI assembly steps are typically seen as sequential, but the exact order in which small subunits and auxiliary assembly factors are added after formation of the PsaA/PsaB heterodimer (Wostrikoff et al., 2004) is still largely unknown.

Previous studies have proposed that binding of the stromal/cytoplasmic subunits PsaC, PsaD, and PsaE is preceded by coordination of the  $F_X$  iron-sulfur cluster (Kanda et al., 2021) into the early-formed PsaA/PsaB heterodimer and is followed, notably in plants, by incorporation of the small TM subunits PsaL, PsaI, and PsaH (Rolo et al., 2024). In cyanobacteria, it has been proposed that PsaK is incorporated at the latest stage of PSI monomer assembly (Dühring et al., 2007) and that the presence of PsaM (Naithani et al., 2000) and especially PsaL (Dühring et al., 2007) is required for formation of the stable PSI trimer (Figure 1A). However, this model is challenged by the observation that the small TM subunits can still be incorporated in the absence of cytoplasmic subunits in a rubredoxin A knockout mutant of *Synechococcus* (Shen et al., 2002). To provide new insights into PSI biogenesis, we analyzed the structure of a monomeric PSI complex isolated from the  $\Delta\text{PsaC}$  mutant of the cyanobacterium *Synechocystis* sp. PCC 6803 (hereafter *Synechocystis*). Using single-particle cryoelectron microscopy (cryo-EM), its structure

was resolved at an exceptionally high resolution of 1.83 Å, providing new insight into PSI assembly.

We generated a *Synechocystis* mutant lacking the *psaC* gene and expressing FLAG-tagged PsaA (FLAG-*psaA*/ $\Delta\text{psaC}$ ; Supplemental Figure 1). Clear native polyacrylamide gel electrophoresis (CN-PAGE) indicated a prevalence of monomeric PSI in membranes of the mutant, with some trimeric form present, whereas the trimeric form predominated over the monomeric form in the control line (FLAG-*psaA*) (Figure 1B; Supplemental Figure 2). This result showed that depletion of PsaC substantially impairs PSI trimerization. Using FLAG affinity pull-down, we isolated FLAG-PSI $\Delta\text{C}$  and control FLAG-PSI preparations. Their absorption spectra showed similar overall pigment contents (Supplemental Figure 3A), and their light-dark absorption difference spectra also demonstrated similar primary charge-separation activity (Supplemental Figure 3B). Two-dimensional CN/SDS-PAGE and mass spectrometry (MS) confirmed the presence of PsaC, PsaD, and PsaE in FLAG-PSI but their complete absence in FLAG-PSI $\Delta\text{C}$  (Figure 1B; Supplemental Tables 1 and 2). By contrast, PsaF and PsaK1 were present in monomers and trimers of both preparations (Supplemental Table 3). PsaL was identified by MS in trimeric PSI from both preparations and in the FLAG-PSI monomer but only in a small fraction of the FLAG-PSI $\Delta\text{C}$  monomer (Supplemental Table 3). This finding was confirmed by 2D blot analysis (Supplemental Figure 4). Bands corresponding to PsaI, PsaJ, and PsaM were not detected because of their small size and poor gel resolution (Figure 1B). Moreover, these minisubunits yield no or a very limited number of mostly hydrophobic and barely detectable tryptic peptides, which also explains their absence in the analysis of individual native PSI bands from CN gels (Supplemental Table 3).

To determine the three-dimensional (3D) structure of the PSI complex lacking PsaC and to identify all associated subunits, the FLAG-PSI $\Delta\text{C}$  preparation was analyzed by single-particle cryo-EM. For the reference and template model, we used the *Synechocystis* trimeric PSI complex resolved by Malavath et al. (2018) (PDB: 5OY0; referred to as mature PSI). We collected 9991 movies (Supplemental Figure 5, Supplemental Table 4), which enabled us to obtain 334 941 particles used to reconstruct the structure. The well-defined density enabled us to build an atomic model of the monomeric FLAG-PSI $\Delta\text{C}$  complex (for simplicity, PSI $\Delta\text{C}$  hereafter) with a global resolution of 1.83 Å, although the dimeric and trimeric FLAG-PSI $\Delta\text{C}$  complexes were not resolved, likely because of their low abundance



in the preparation. The density in the center of PSIΔC revealed high-resolution details, enabling the clear identification of pigments and their puckering state, correct rotameric angles of protein side chains, and precise conformations and orientations of Chl molecules (Supplemental Figures 6 and 7). The complex consisted of seven protein subunits: PsaA, PsaB, PsaF, and PsaK, together with PsaI, PsaJ, and PsaM, which were not detected in the proteomic analysis (Figure 1C). We clearly identified the PsaK1 paralog in PSIΔC, whereas the mature PSI reference model (PDB: 5OY0) contained PsaK2 (Figure 1D). However, the lower resolution reported in (Malavath et al. 2018) may have limited the ability to clearly identify the correct paralog, leaving open the possibility that PDB: 5OY0 also contained PsaK1. In agreement with Toporik et al. (2019), our data support predominant incorporation of PsaK1, which stabilizes Chl 4003 with an  $\alpha$  helix through the F51 residue. By contrast, PsaK2 has a loop in this region, which would cause structural clashes in the mature PSI complex (Figure 1D). Furthermore, the absence of PsaD, which is the main interactor of PsaL at the cytoplasmic side of PSI, with up to seven contact points (Supplemental Figure 8), renders the interaction of PsaL with monomeric PSIΔC less stable than that with the complete PSI monomer (Supplemental Figure 8). This likely explains the absence of PsaL in the PSIΔC structure.

We modeled 93 Chls and 20 carotenoids in our PSIΔC structure (Supplemental Figure 7; Supplemental Table 5), along with reaction center components like P700, auxiliary Chls, and phyloquinones, organized identically to those in mature PSI (Figure 1E). In PSIΔC, the  $F_X$  cluster had weaker density, likely due to partial occupancy, and contained only two iron ions and four sulfide ions (Supplemental Figure 9A). In mature PSI, the  $F_X$  cluster comprises four sulfide anions and four ferrous cations coordinated by four cysteine residues: Cys574 (Fe3) and Cys583 (Fe2) of PsaA, and Cys556 (Fe4) and Cys565 (Fe1) of PsaB (Figure 1F; Supplemental Figure 9B). In PSIΔC, Fe1 is present but is not coordinated by its usual Cys565 residue from PsaB, which is displaced and replaced by a water molecule (Figure 1F). Instead, Cys565 interacts with the carbonyl of Cys556, and its thiol group interacts with the S2 sulfide (Figure 1F; Supplemental Figure 9C). Fe2 is absent, although its coordinating cysteine from PsaA is correctly positioned (Figure 1F). Fe3 is present and properly coordinated, similar to that in the mature complex, but Fe4 is absent, with its coordinating cysteine from PsaB displaced by 2.8 Å (Figure 1F). In the absence of PsaC, the observed loss of two irons may be the result of oxidation or another modification that occurred during purification of the complex and/or its embedding into the EM grid. Nevertheless, we believe that it is a consequence of the unavailability of Cys residues of PsaB, related to the disorder of

the neighboring PsaB region (residues 573–585) (Figure 1G). This region normally includes a  $\beta$ -turn (577–581) stabilized by interactions with PsaC and PsaE (Figure 1G; Supplemental Figure 9D), which ensures the correct positioning of Cys556 and Cys565 of PsaB to fully coordinate the complete  $F_X$  cluster. This interpretation is supported by the observation of incomplete [3Fe–4S] clusters in cells of a C565S PsaC *Synechocystis* mutant and a similar *Synechococcus* mutant (Warren et al., 1993; Pérez et al., 2018). Conversely, lack of  $F_X$  has been shown to prevent assembly of the cytoplasmic subunits (Shen et al., 2002). Together, our data and previous studies thus suggest an intrinsically encoded mechanism for  $F_X$  insertion and stabilization, working through synchronized structural rearrangement of PsaB, which accompanies the binding of the cytoplasmic subunits.

In conclusion, we found that the small TM subunits of cyanobacterial PSI can associate with the PsaA/PsaB heterodimer during the assembly process, independently of the presence of cytoplasmic subunits. PsaC is essential for binding of the other two cytoplasmic subunits and also contributes to recruiting PsaL, which strongly interacts with PsaD and also facilitates trimer formation. PsaC is also important for formation of the correct  $F_X$  binding site, which requires conformational rearrangements of PsaB induced by PsaC binding. Without these rearrangements, the resulting  $F_X$  cluster remains incomplete and lacks two iron ions. Our findings allow for alternative scenarios of PSI assembly (alongside the prevailing model shown in Figure 1A), in which the simultaneous building of the  $F_X$  cluster and the association of PsaC (and other cytoplasmic subunits) with the PsaA/PsaB heterodimer occur after, or concurrently with, the binding of most of the small TM subunits.

## DATA AVAILABILITY

Atomic coordinates of PSIΔC have been deposited in the Protein Data Bank under accession code 8ZWB. The EM density map of PSIΔC has been deposited in the Electron Microscopy Data Bank under accession code EMD-60522.

## FUNDING

We are very grateful to the KAUST Opportunity Fund (A.N., J.K., and R.S., project RFS-OFP2023-5561), the Czech Grant Agency (J.K.; project no. 24-10227S), ERC (J.K.; project no. 854126), the Ministry of Education, Youth and Sports (R.S. and P.N.; OP JAK project no. CZ.02.01.01/00/22\_008/0004624), and Czech Academy of Sciences (D.B.; institutional support RVO:60077344) for funding.

## ACKNOWLEDGMENTS

We thank Jan Pilný, Eva Prachová, and Kateřina Novotná for excellent technical support. We thank the cryo-EM facility at KAUST for their assistance with data collection. The authors declare no competing interests.

**(D)** Detailed analysis of the PsaK subunit in PSIΔC compared with mature PSI. Left: model and density of PsaK1 apoprotein from PSIΔC. Middle: superposition of PsaK1 and PsaK2 holoproteins from PSIΔC and mature PSI, respectively. Right: close-up view of the Chl-a 4003 region of PSIΔC. The models of PSIΔC (cyan) and PSI (pink) were superposed, and the density from PSIΔC is shown.

**(E)** Components of the electron transport chain in PSIΔC. The cofactors are colored to indicate their association with PsaA (green) or PsaB (red). Chls of the electron transport chain are arranged in three pairs referred to as P700, Acc, and A0. Phyloquinones are labeled as  $Q_k$  and the iron-sulphur cluster as  $F_X$ .

**(F)** Superposition of PSIΔC (green and red) and mature PSI (gray), showing  $F_X$  cluster coordination by cysteine residues. Only the iron atoms and their numbers in  $F_X$  of mature PSI are shown in gray.

**(G)** Wide view of the  $F_X$  coordination site. Models of PSIΔC and PSI are superposed. The PsaB loop (light gray), PsaE (gray), PsaC (cyan), and the  $F_X$  cluster (transparent) from mature PSI and the PsaB loop (red) from PSIΔC are shown. For both models, the Cys556 and Cys565 residues are shown. The red circle indicates the virtual clash between PsaB from PSIΔC and PsaC from the mature PSI.



## AUTHOR CONTRIBUTIONS

A.N. and J.K. designed the study; S.G. and M.T. constructed the strains; S.G., R.S., D.S., and J.K. prepared and characterized the PSI complexes; D.B. recorded and analyzed the light–dark absorption difference spectra; A.N. processed the structural data; Q.C. built the model and analyzed the structure; A.A.-A. collected the cryo-EM data; M.L. and P.K. analyzed protein bands in the gel; P.N. and M.Z. performed MS analysis of the FLAG–PSIΔC preparation; and Q.C., S.G., A.N., J.K., and R.S. jointly prepared the figures and wrote the manuscript.

## SUPPLEMENTAL INFORMATION

Supplemental information is available at *Plant Communications Online*.

Received: June 8, 2025

Revised: August 6, 2025

Accepted: August 21, 2025

Published: August 25, 2025

**Quentin Charras Ferroussier<sup>1,6</sup>,  
Sadanand Gupta<sup>2,3,6</sup>, Martin Tichý<sup>2</sup>,  
Ashraf Al-Amoudi<sup>1</sup>, Martin Lukeš<sup>2</sup>,  
Daniel Štipl<sup>2,3</sup>, Peter Koník<sup>2,3</sup>, David Bína<sup>3,5</sup>,  
Marek Zákopčaník<sup>4</sup>, Petr Novák<sup>4</sup>,  
Roman Sobotka<sup>2,3</sup>, Josef Komenda<sup>2,\*</sup> and  
Andreas Naschberger<sup>1,\*</sup>**

<sup>1</sup>King Abdullah University of Science and Technology (KAUST), Biological and Environmental Science and Engineering Division, 23955 Thuwal, Saudi Arabia

<sup>2</sup>Centre Algatech, Institute of Microbiology of the Czech Academy of Sciences, 379 01 Třeboň, Czech Republic

<sup>3</sup>Faculty of Science, University of South Bohemia, 370 05 České Budějovice, Czech Republic

<sup>4</sup>Laboratory of Structural Biology and Cell Signaling, Institute of Microbiology of the Czech Academy of Sciences, 14220 Prague, Czech Republic

<sup>5</sup>Institute of Plant Molecular Biology, Biology Centre of the Czech Academy of Sciences, 370 05 České Budějovice, Czech Republic

<sup>6</sup>These authors contributed equally to this article.

\*Correspondence: Josef Komenda ([komenda@alga.cz](mailto:komenda@alga.cz)), Andreas Naschberger ([andreas.naschberger@kaust.edu.sa](mailto:andreas.naschberger@kaust.edu.sa))  
<https://doi.org/10.1016/j.xplc.2025.101493>

## REFERENCES

- Caspy, I., Borovikova-Sheinker, A., Klaiman, D., Shkolnisky, Y., and Nelson, N. (2020). The structure of a triple complex of plant photosystem I with ferredoxin and plastocyanin. *Nat. Plants* **6**:1300–1305.
- Dürring, U., Ossenbühl, F., and Wilde, A. (2007). Late Assembly Steps and Dynamics of the Cyanobacterial Photosystem I. *J. Biol. Chem.* **282**:10915–10921.
- Kanda, T., Saito, K., and Ishikita, H. (2021). Electron Acceptor–Donor Iron Sites in the Iron–Sulfur Cluster of Photosynthetic Electron-Transfer Pathways. *J. Phys. Chem. Lett.* **12**:7431–7438.
- Malavath, T., Caspy, I., Netzer-El, S.Y., Klaiman, D., and Nelson, N. (2018). Structure and function of wild-type and subunit-depleted photosystem I in *Synechocystis*. *Biochim. Biophys. Acta. Bioenerg.* **1859**:645–654.
- Naithani, S., Hou, J.M., and Chitnis, P.R. (2000). Targeted inactivation of the *psaK1*, *psaK2* and *psaM* genes encoding subunits of Photosystem I in the cyanobacterium *Synechocystis* sp. PCC 6803. *Photosynth. Res.* **63**:225–236.
- Naschberger, A., Mosebach, L., Tobiasson, V., Kuhlert, S., Scholz, M., Perez-Boerema, A., Ho, T.T.H., Vidal-Meireles, A., Takahashi, Y., Hippler, M., and Amunts, A. (2022). Algal photosystem I dimer and high-resolution model of PSI-plastocyanin complex. *Nat. Plants* **8**:1191–1201.
- Pérez, A.A., Ferlez, B.H., Applegate, A.M., Walters, K., He, Z., Shen, G., Golbeck, J.H., and Bryant, D.A. (2018). Presence of a [3Fe–4S] cluster in a PsaC variant as a functional component of the photosystem I electron transfer chain in *Synechococcus* sp. PCC 7002. *Photosynth. Res.* **136**:31–48.
- Rolo, D., Schöttler, M.A., Sandoval-Ibáñez, O., and Bock, R. (2024). Structure, function, and assembly of PSI in thylakoid membranes of vascular plants. *Plant Cell* **36**:4080–4108.
- Shen, G., Zhao, J., Reimer, S.K., Antonkine, M.L., Cai, Q., Weiland, S.M., Golbeck, J.H., and Bryant, D.A. (2002). Assembly of Photosystem I: I. INACTIVATION OF THE *rubA* GENE ENCODING A MEMBRANE-ASSOCIATED RUBREDOXIN IN THE CYANOBACTERIUM *SYNECHOCOCCUS* SP. PCC 7002 CAUSES A LOSS OF PHOTOSYSTEM I ACTIVITY. *J. Biol. Chem.* **277**:20343–20354.
- Toporik, H., Li, J., Williams, D., Chiu, P.-L., and Mazor, Y. (2019). The structure of the stress-induced photosystem I–LsiA antenna supercomplex. *Nat. Struct. Mol. Biol.* **26**:443–449.
- Warren, P.V., Smart, L.B., McIntosh, L., and Golbeck, J.H. (1993). Site-directed conversion of cysteine-565 to serine in PsaB of photosystem I results in the assembly of iron-sulfur [3Fe–4S] and iron-sulfur [4Fe–4S] clusters in Fx. A mixed-ligand iron-sulfur [4Fe–4S] cluster is capable of electron transfer to FA and FB. *Biochemistry* **32**:4411–4419.
- Wostrikoff, K., Girard-Bascou, J., Wollman, F.-A., and Choquet, Y. (2004). Biogenesis of PSI involves a cascade of translational autoregulation in the chloroplast of *Chlamydomonas*. *EMBO J.* **23**:2696–2705.

**Supplemental information**

**High-resolution structural analysis of the cyanobacterial photosystem  
I complex reveals independent incorporation of small transmembrane  
and cytoplasmic subunits**

**Quentin Charraŕs Ferroussier, Sadanand Gupta, Martin Tichý, Ashraf Al-Amoudi, Martin  
Lukeš, Daniel Štipl, Peter Koník, David Bína, Marek Zákopčaník, Petr Novák, Roman  
Sobotka, Josef Komenda, and Andreas Naschberger**

## **Supplemental Information:**

**Supplemental Figure 1. Construction of the *Synechocystis* mutants.**

**Supplemental Figure 2. Analysis of membranes from *Synechocystis* strains expressing the FLAG–PsaA subunit instead of PsaA and either containing PsaC (FLAG–*psaA*) or lacking PsaC (FLAG–*psaA*/Δ*psaC*).**

**Supplemental Figure 3. Characterization of the isolated FLAG–PSI and FLAG–PSIΔC preparations.**

**Supplemental Figure 4. 2D Western blot analysis of FLAG–affinity purified pull-downs isolated from *Synechocystis* strains expressing Flag–PsaA instead of PsaA and either containing (FLAG–PSI) or lacking PsaC (FLAG–PSIΔC).**

**Supplemental Figure 5. (A) Cryo–EM data processing, (B) local resolution, and (C) angular distribution, and Fourier shell correlation plot.**

**Supplemental Figure 6. High resolution features of pigments and protein parts in the protein core of the PSIΔC.**

**Supplemental Figure 7. Pigment binding sites in the PSIΔC and HPLC analysis of pigments extracted from the isolated PSI preparations.**

**Supplemental Figure 8. Main protein–protein interactions established by PsaL with other subunits of mature PSI.**

**Supplemental Figure 9: Organization of the F<sub>x</sub> cluster in PSIΔC and mature PSI (5OY0).**

**Supplemental Table 1. Mass spectrometric identification of protein bands designated in the 2D gel analysis of the FLAG–PSI preparation in Fig. 1B.**

**Supplemental Table 2. List of the most abundant 40 proteins identified by MS in the FLAG–PSIΔC preparation.**

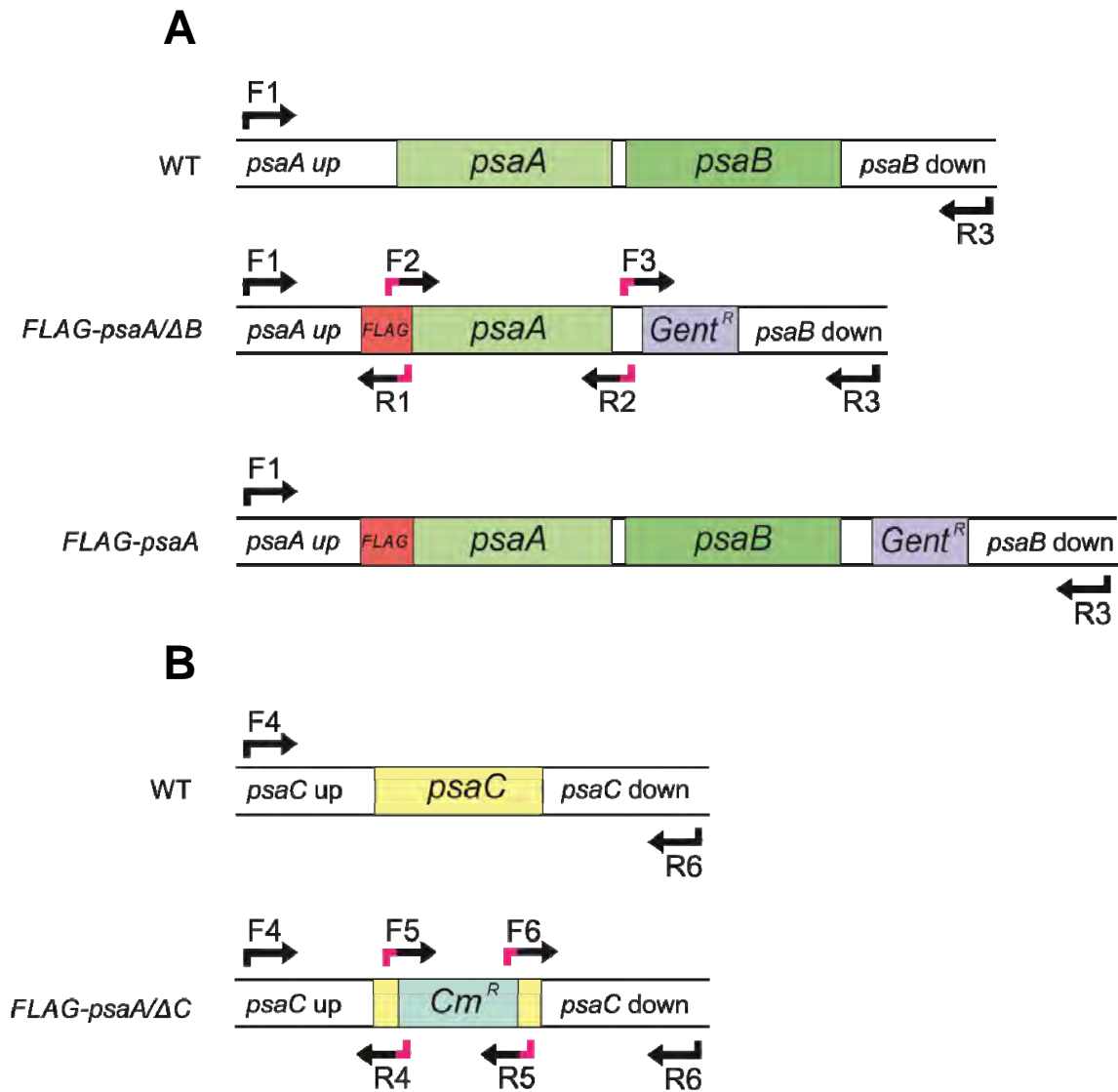
**Supplemental Table 3. Mass spectrometric (MS) and Western blot (WB) identification of proteins in trimeric and monomeric PSI complexes of FLAG–PSI and FLAG–PSIΔC preparations separated in the CN gel shown in Supplemental Figure 4.**

**Supplemental Table 4. Cryo–EM single particle analysis. Summary of the data collection, refinement, and validation statistics of PSIΔC (EMDB-60522) (PDB 8ZWB).**

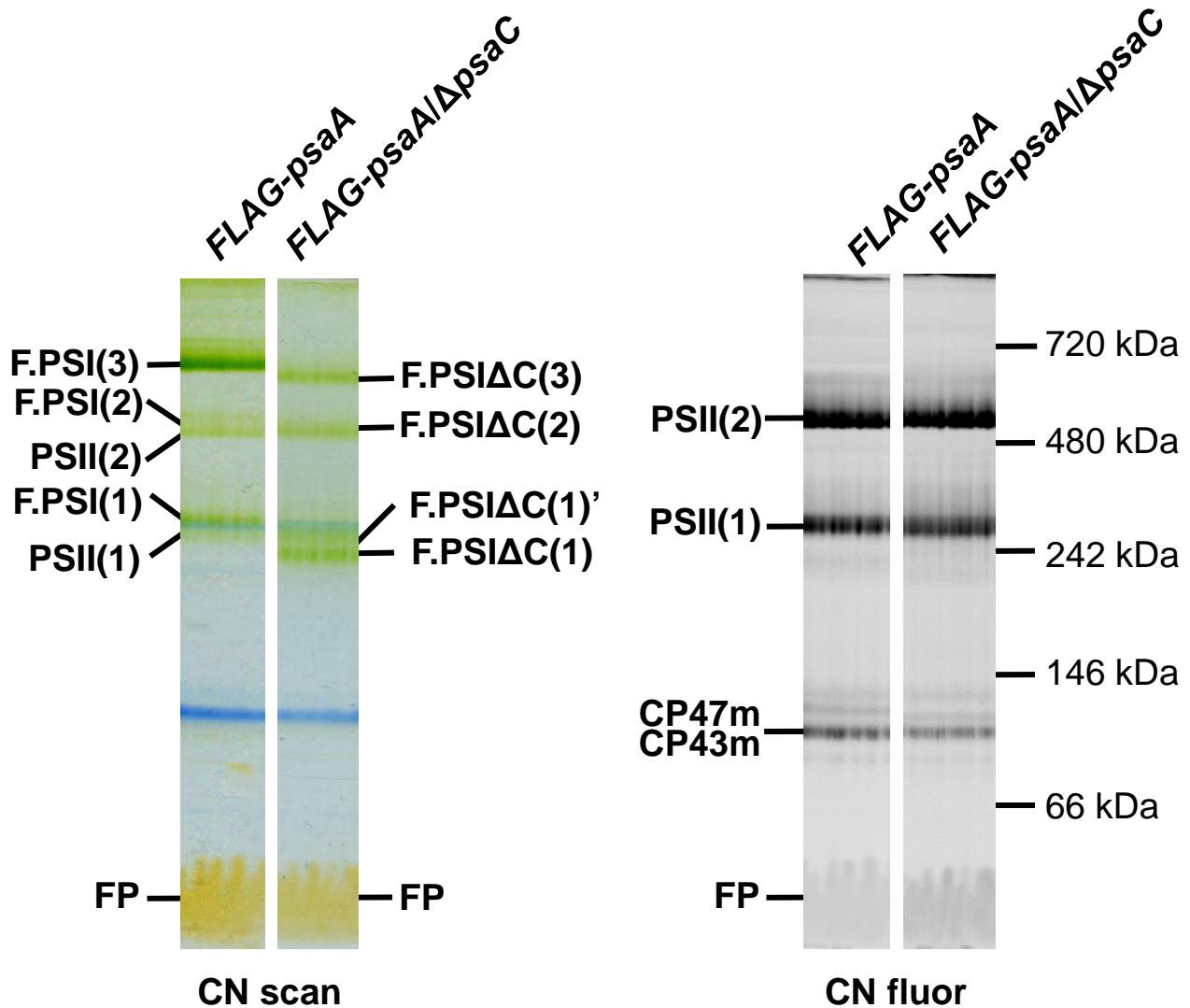
**Supplemental Table 5. Pigment and lipids composition of each PSIΔC subunit based on the cryo–EM structure.**

**Supplemental Table 6. List of primers used for constructing mutants used in the study (see Supplemental Figure 1).**

**Methods**



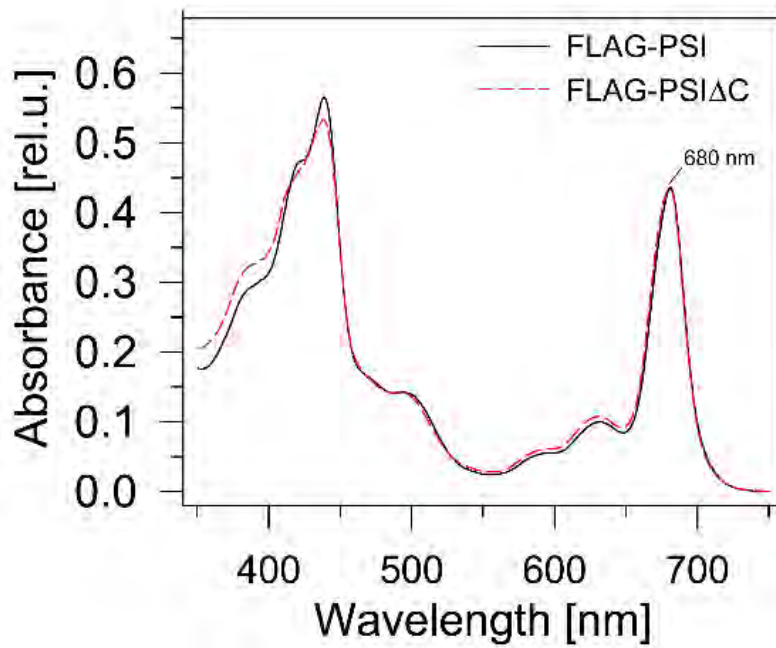
**Supplemental Figure 1. Construction of the *Synechocystis* mutants.** (a) The *FLAG-psaA/ΔpsaB* strain was prepared by replacement of the original *psaA* and *psaB* genes by a construct containing *psaA* gene with an N-terminally attached sequence encoding 1xFLAG and gentamycin resistance cassette downstream. The *FLAG-psaA* strain was prepared by the insertion of the original *psaB* gene between *FLAG-psaA* gene and gentamycin resistance cassette and selecting for autotrophy. (b) The *FLAG-psaA/ΔpsaC* strain was prepared by replacing most of the original *psaC* gene by the chloramphenicol resistance cassette. F1-F6 and R1-R6 designate primers described in Supplemental Table 6.



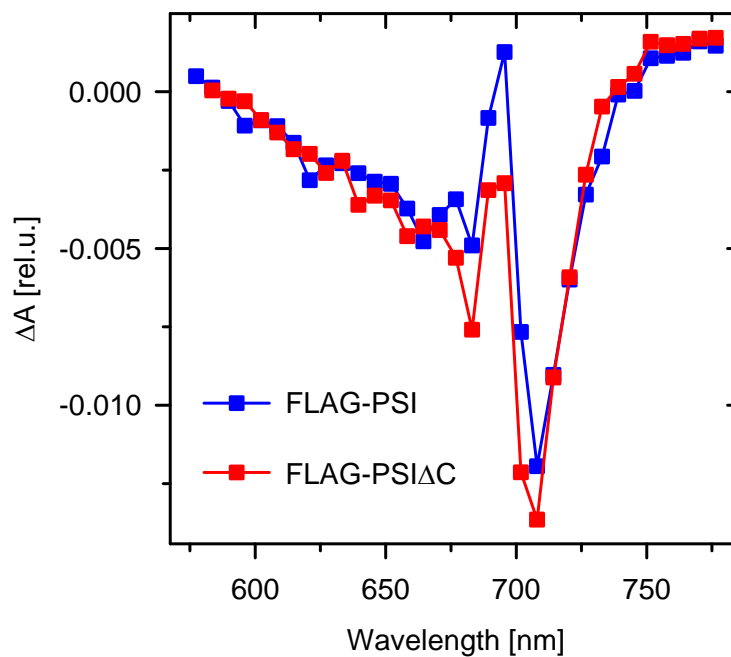
**Supplemental Figure 2. Analysis of membranes from *Synechocystis* strains expressing the FLAG–PsaA subunit instead of PsaA and either containing PsaC (*FLAG–psaA*) or lacking PsaC (*FLAG–psaA/ΔpsaC*).** The complexes were separated by CN PAGE and the gel was photographed (CN scan) and scanned for Chl fluorescence (CN fluor). Note the different PSI and identical PSII mobilities of complexes in the control and in the PsaC–lacking strain. Designation of complexes: F.PSI(3), F.PSI(2) and F.PSI(1), FLAG-tagged trimeric, dimeric and monomeric Photosystem I; F.PSI(3) $\Delta$ C and F.PSI(2) $\Delta$ C, FLAG-tagged trimeric and dimeric Photosystem I lacking PsaC; F.PSI(1) $\Delta$ C' and F.PSI(1) $\Delta$ C, FLAG-tagged monomeric Photosystem I lacking PsaC and containing PsaL, respectively; PSII(2) and PSII(1), dimeric and monomeric Photosystem II; CP47m and CP43m, unassembled CP47 and CP43 modules; FP, free pigments. The loading of the membranes was based on the same OD<sub>750nm</sub> corresponding to 5  $\mu$ g of chlorophyll for *FLAG–psaA* strain and 4  $\mu$ g of chlorophyll for *FLAG–psaA/ΔpsaC* strain.



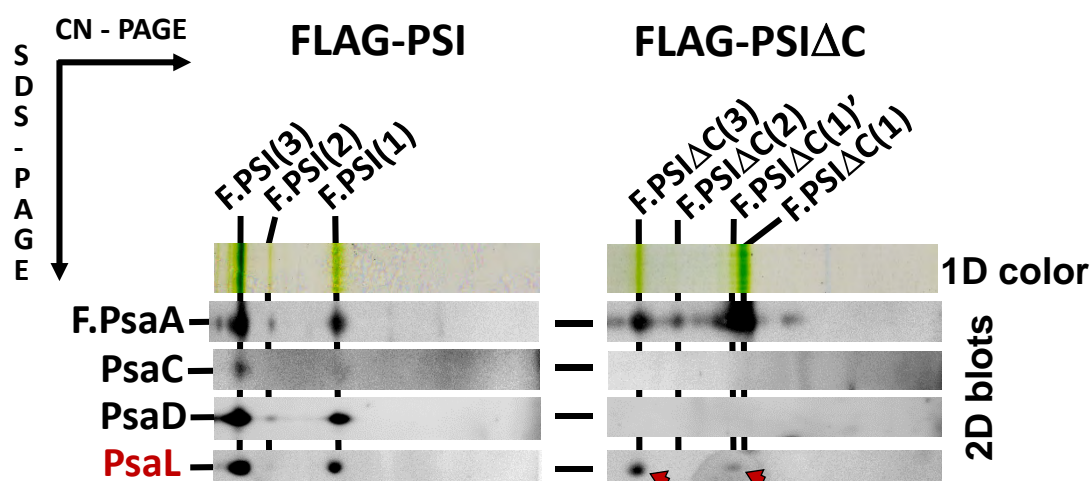
A



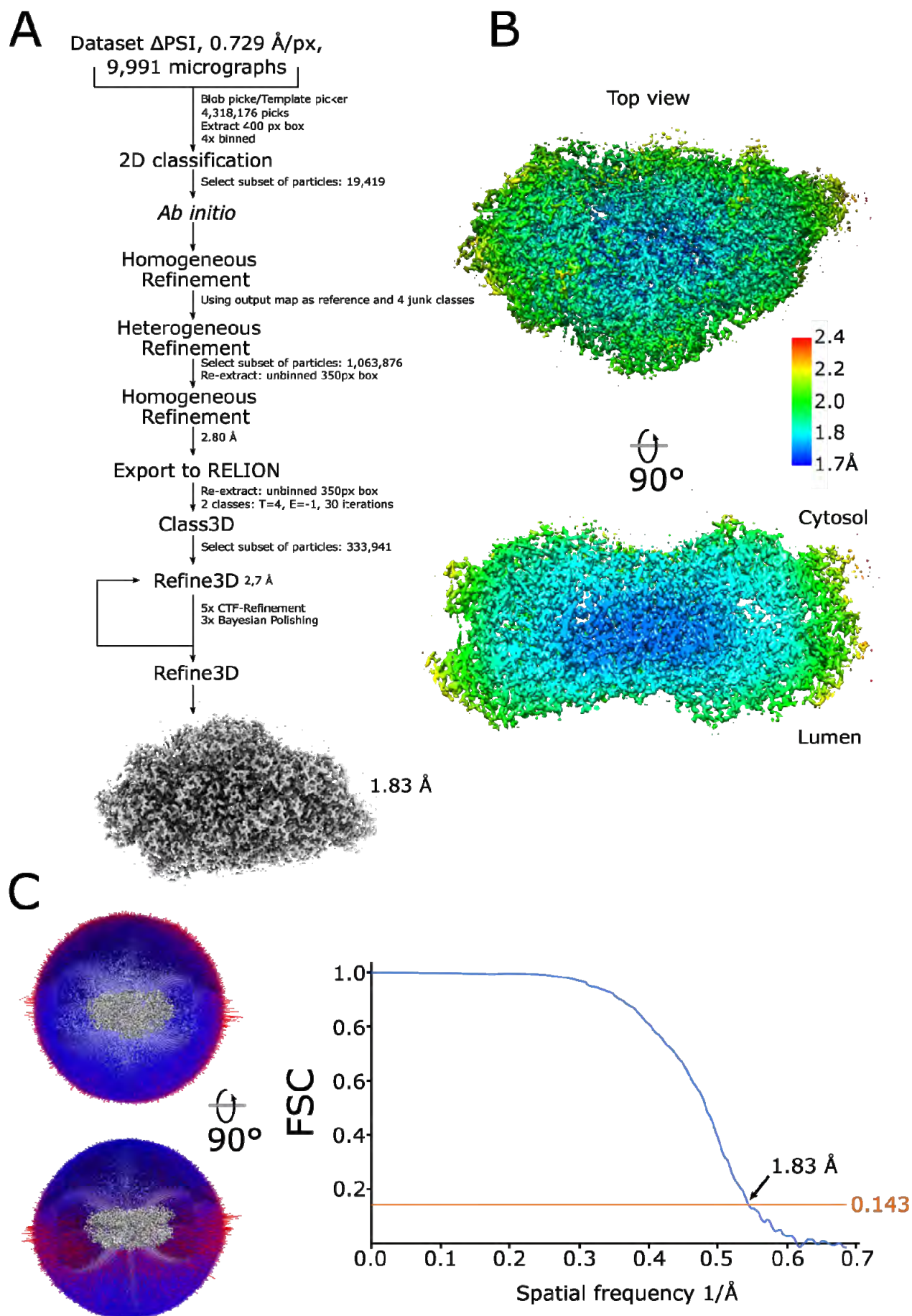
B



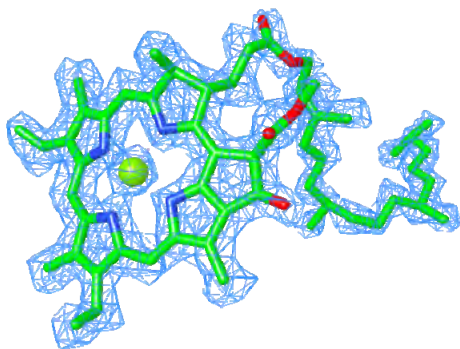
**Supplemental Figure 3. Characterization of the isolated FLAG-PSI and FLAG-PSI $\Delta$ C preparations. (A)** Absorption spectra of FLAG-affinity purified pull-downs normalized to the 680 nm peak of Chl. **(B)** Difference (light-dark) absorption spectra measured at the end of the 3 s-long illumination of the FLAG-affinity purified pull-downs using blue LED (maximum 470 nm) in the presence of 5 mM sodium ascorbate. The spectra are normalized to the 680 nm peak of Chl.



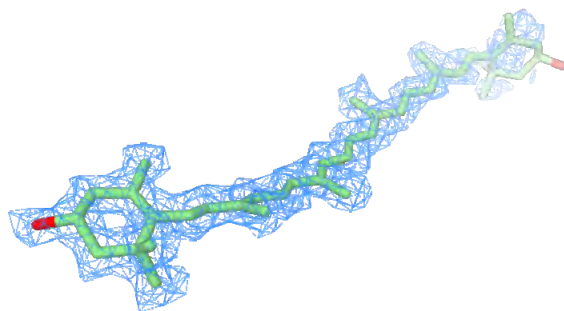
**Supplemental Figure 4. 2D Western blot analysis of FLAG–affinity purified pull-downs isolated from *Synechocystis* strains expressing Flag-PsaA instead of PsaA and either containing (FLAG–PSI) or lacking PsaC (FLAG–PSIΔC).** Preparations were analyzed by CN PAGE in the first dimension, the native gel was photographed (1D color), the lanes were cut and heated in 2% SDS at 50 °C for 20 min. After SDS–PAGE in the 2nd dimension the gel was stained with SYPRO Orange, electroblotted and the blot was sequentially probed by antibodies specific for PsaL, PsaC, PsaD and FLAG. Designation of complexes as in Fig. 1. The signals of PsaL in the trimer and minor monomer of FLAG–PSIΔC are designated by red arrow. Each loaded sample contained 5 μg of Chl.



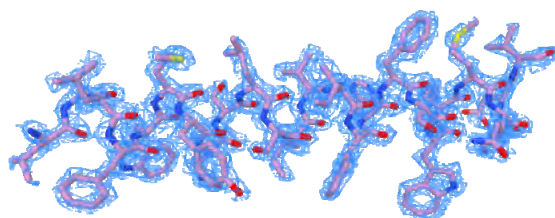
**Supplemental Figure 5.** (A) Cryo EM data processing, (B) local resolution, and (C) angular distribution, and Fourier shell correlation plot.



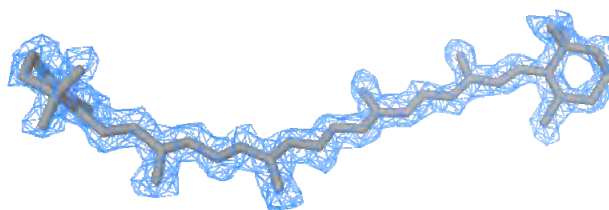
Chlorophyll a (PsaA CLA801)



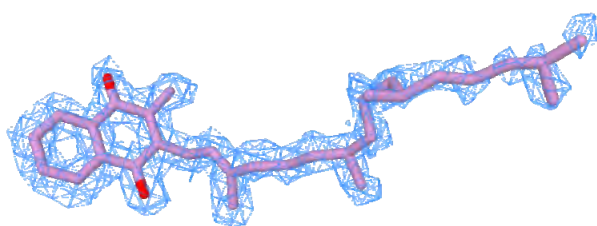
Zeaxanthin (PsaB XXX 868)



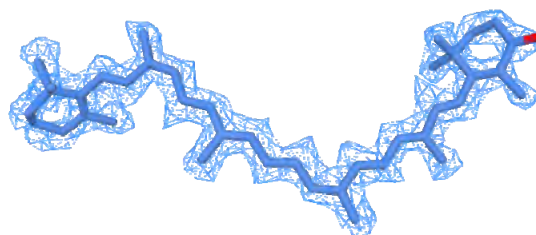
PsaA (593-617)



$\beta$ -Carotene (PsaF BCR 203)



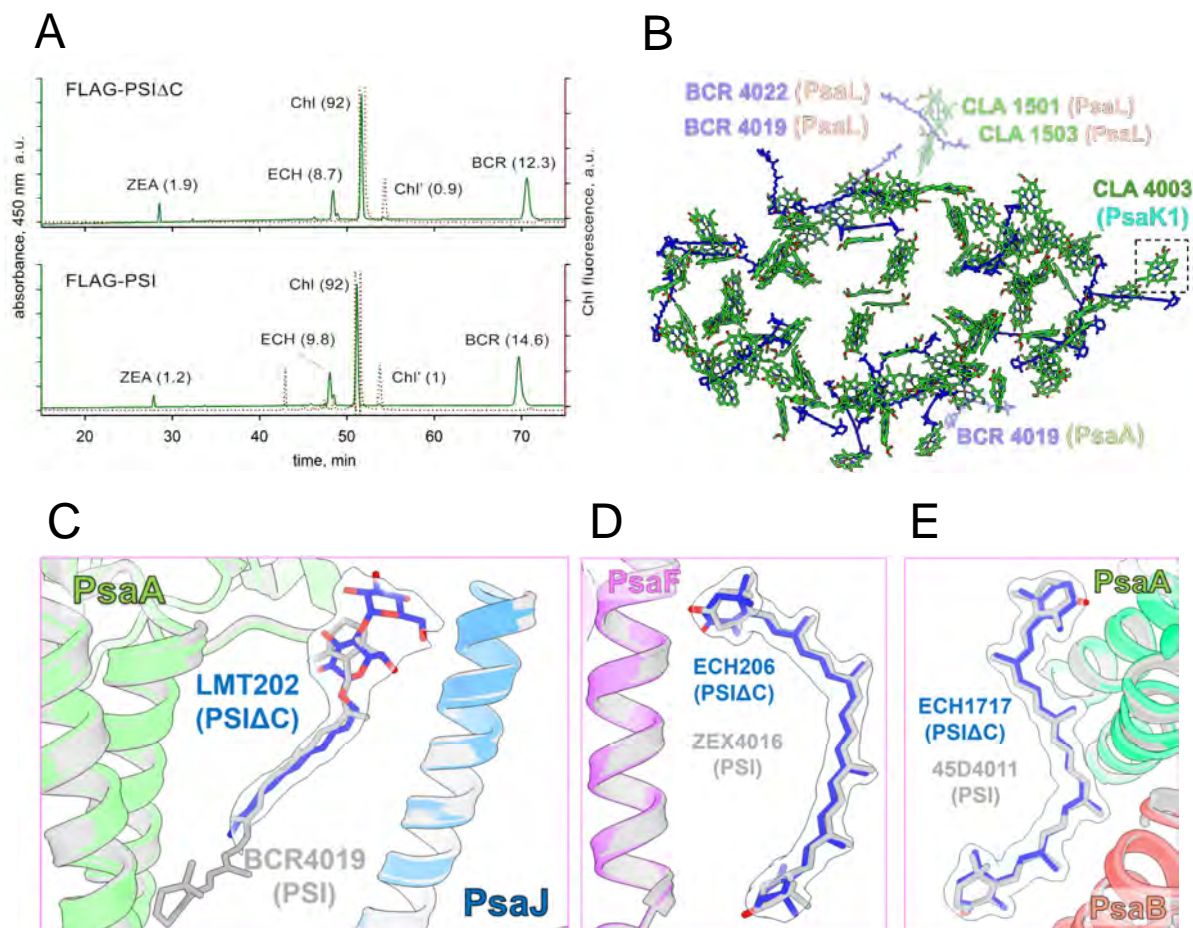
Phylloquinone (PsaA PQN804)



Echinenone (PsaA ECH 851)

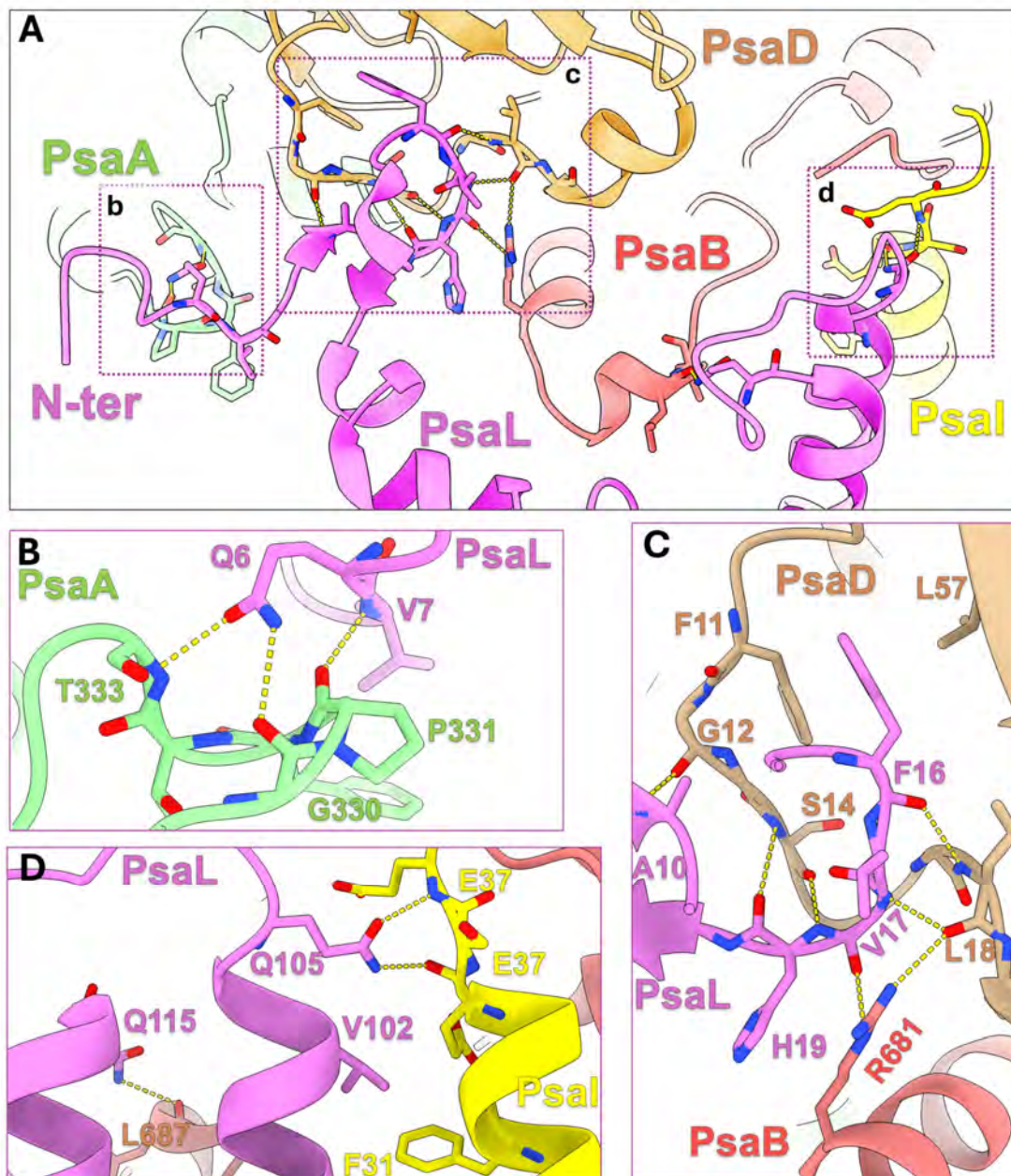
**Supplemental Figure 6. High resolution features of pigments and protein parts in the protein core of the PSI $\Delta$ C.**



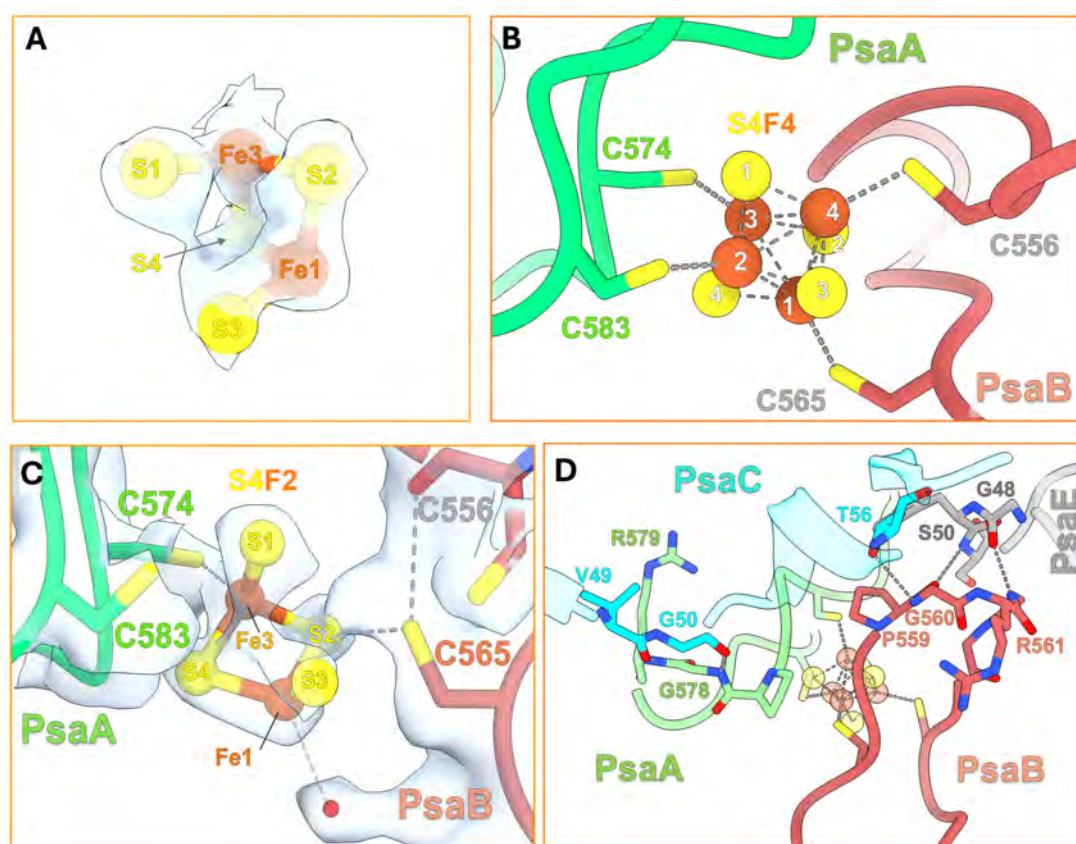


**Supplemental Figure 7. Pigment binding sites in the PSIΔC and HPLC analysis of pigments extracted from the isolated PSI preparations. (A)** HPLC analysis of pigments. FLAG-PSIΔC and the control FLAG-PSI pulldowns that were isolated using FLAG affinity chromatography from strains expressing FLAG-PsaA instead of PsaA and containing or lacking PsaC. The extracted carotenoids and Chl were separated by HPLC and detected by a diode-array detector (DAD) at 450 nm (solid green light). Although the C<sup>13</sup>-epimer of chlorophyll a (Chl') can be detected using absorbance, its quantification is not precise due to its too weak signal, specifically when compared to the absorbance of Chl. However, the fluorescence emission of the Chl' epimer at 670 nm can be detected using more sensitive fluorescence detector after excitation at 435 nm (dotted red line). Molar stoichiometries of the identified pigments in FLAG-PSIΔC are shown in parentheses (normalized to 92 Chls and 1 Chl' in FLAG-PSI) and these values represent the means of three technical replicates; standard deviations were below 10%. ZEA – zeaxanthin, ECH – echinenone, BRC – β-carotene, a.u. – arbitrary units. **(B)** The pigment network of PSIΔC. Chlorophylls are colored green and carotenoids blue. Chla 4003 (PsaK) absent in PSI is marked with a dashed square. Two Chls (CLA 1501 and 1503) and two β-carotenes (BCR 4019 and 4022) normally bound to PsaL and one β-carotene bound to PsaA (BCR 4019) are absent in PSIΔC and are colored transparent. **(C-E)** Superposition of PSIΔC and the mature model showing different co-factor occupations at specific sites. The mature PSI is coloured grey. Specifically, one β-carotene in the vicinity of PsaJ was lost and replaced by the dodecyl-β-D-maltoside molecule (LMT202). Moreover, two carotenoids were modelled as echinenones, whereas in the structure of Malavath *et al.* (2018), these densities were modelled as zeaxanthin and an isomer of canthaxanthin.





**Supplemental Figure 8. Main protein–protein interactions established by PsaL with other subunits of mature PSI.** (A) Cytoplasmic view of the PsaL extramembrane region forming protein–protein interaction with PsaA, PsaB, PsaD and PsaL. (B–D) close view of the protein–protein interactions marked with dotted rectangles in (A). Figures are based on previously published PSI structure (Malavath et al., 2018; PDB 5OY0).



**Supplemental Figure 9: Organisation of the  $F_x$  cluster in  $PSI\Delta C$  and the mature PSI (5OY0).** (A) Model and density of the  $F_x$  cluster from the  $PSI\Delta C$ . (B) Coordination of the  $F_x$  cluster with cysteine residues from PsaA and PsaB in the mature PSI. (C) Coordination of the  $F_x$  cluster from the  $PSI\Delta C$  with cysteine residues from PsaA and PsaB. The density of the designated atoms and residues is shown. (D) Wide view of the  $F_x$  coordination site. PsaA loop, PsaB loop, PsaE, PsaC and the  $F_x$  cluster from the mature PSI are shown in light green, red, dark grey, light cyan and transparent orange-yellow, respectively. Interactions between residues are shown.

**Supplemental Table 1. Mass spectrometric identification of protein bands designated in the 2D gel analysis of the FLAG–PSI preparation in Fig. 1B.**

Accession number	Mass spectrometric analysis			
	Length (AA)	Size (Da)	Sequence coverage (%)	Intensity
<b>PsaA</b> P29254	751	82,950	20	38,597,000
<b>PsaB</b> P29255	731	81,292	12	16,375,000
<b>PsaC</b> P32422	81	8,828	49	3,492,300
<b>PsaD</b> P19569	141	15644	90	78,489,000
<b>PsaF</b> P29256	165	18,249	48	47,937,000
<b>PsaL</b> P37277	157	16624	11	1,035,500
<b>PsbE</b> P12975	74	8145	96	29,097,000
<b>PsaK1</b> P72712	86	8,644	20	422,860
<b>PsaK2</b> P74564	90	9,306	10	2,644,000

LC-MS/MS analysis was performed on an UltiMate 3000 UHPLC (Thermo Fisher Scientific) on-line coupled to a timsTOF Pro (Bruker Daltonics) mass spectrometer. The identifications were quantified using IBAQ quantification mode.

**Supplemental Table 2. List of the most abundant 40 proteins identified by MS in the FLAG-PSI $\Delta$ C preparation.**

Accession numbers	Protein name	No of peptides	Intensity
<a href="#">P29256 PSAF SYN3</a>	<b>Photosystem I subunit Psaf</b>	18	6.18E+05
<a href="#">P29254 PSAA SYN3</a>	<b>Photosystem I subunit Psaa</b>	24	3.17E+05
<a href="#">P29255 PSAB SYN3</a>	<b>Photosystem I subunit Psab</b>	16	2.66E+05
<a href="#">P05429 PSBB SYN3</a>	Photosystem II subunit PsbB (CP47)	21	1.97E+05
<a href="#">P72804 Y1796 SYN3</a>	<b>Thylakoid membrane protein Slr1796</b>	16	1.81E+05
<a href="#">P74227 EFTU SYN3</a>	Elongation factor Tu	31	1.45E+05
<a href="#">P72991 FTSH3 SYN3</a>	ATP-dependent zinc metalloprotease FtsH3	35	1.25E+05
<a href="#">Q55700 FTSH2 SYN3</a>	ATP-dependent zinc metalloprotease FtsH2	37	1.11E+05
<a href="#">P73437 FTSH4 SYN3</a>	ATP-dependent zinc metalloprotease FtsH4	43	9.33E+04
<a href="#">P73690 YC51L SYN3</a>	<b>Ycf51-like protein Sll1702</b>	5	8.67E+04
<a href="#">P74063 YCF3 SYN3</a>	<b>Photosystem I assembly protein Ycf3</b>	13	7.50E+04
<a href="#">Q55610 SECD SYN3</a>	Protein translocase subunit SecD	23	6.42E+04
<a href="#">Q55544 APCE SYN3</a>	Phycobiliprotein ApcE	48	5.99E+04
<a href="#">P09193 PSBC SYN3</a>	Photosystem II subunit PsbC (CP43)	17	5.72E+04
<a href="#">P72659 PNP SYN3</a>	Polyribonucleotide nucleotidyltransferase	43	5.36E+04
<a href="#">P72986 PSAM SYN3</a>	<b>Photosystem I subunit Psam</b>	4	4.98E+04
<a href="#">P36236 RL1 SYN3</a>	50S ribosomal protein L1 RplA	13	4.36E+04
<a href="#">P73308 RL5 SYN3</a>	50S ribosomal protein L5 RplE	16	4.32E+04
<a href="#">P26527 ATPB SYN3</a>	ATP synthase subunit AtpD	25	4.02E+04
<a href="#">P74071 RS2 SYN3</a>	30S ribosomal protein S2 RpsB	16	3.70E+04
<a href="#">P73317 RL2 SYN3</a>	50S ribosomal protein L2 RplB	13	3.68E+04
<a href="#">P37277 PSAL SYN3</a>	<b>Photosystem I subunit Psal</b>	6	3.68E+04
<a href="#">P73306 RL6 SYN3</a>	50S ribosomal protein L6 RplF	14	3.63E+04
<a href="#">P77969 HEM2 SYN3</a>	Delta-aminolevulinic acid dehydratase HemB	22	3.63E+04
<a href="#">P73334 RPOC2 SYN3</a>	DNA-directed RNA polymerase subunit RpoC2	45	3.61E+04
<a href="#">P73304 RS5 SYN3</a>	30S ribosomal protein S5 RpsE	13	3.45E+04
<a href="#">P42352 RL9 SYN3</a>	50S ribosomal protein L9 RplI	12	3.41E+04
<a href="#">P73318 RL23 SYN3</a>	50S ribosomal protein L23 RplW	9	3.30E+04
<a href="#">P23349 RL7 SYN3</a>	50S ribosomal protein L7/L12 RplL	8	3.28E+04
<a href="#">P80505 G3P2 SYN3</a>	Glyceraldehyde-3-phosphate dihydrogenase 2	20	3.21E+04
<a href="#">P73319 RL4 SYN3</a>	50S ribosomal protein L4 RplD	11	3.20E+04
<a href="#">P73307 RS8 SYN3</a>	30S ribosomal protein S8 RpsH	11	3.14E+04
<a href="#">P73179 FTSH1 SYN3</a>	ATP-dependent zinc metalloprotease FtsH1	36	3.02E+04
<a href="#">P74564 PSAK2 SYN3</a>	<b>Photosystem I reaction center subunit Psak2</b>	6	3.02E+04
<a href="#">P73294 RL13 SYN3</a>	50S ribosomal protein L13 RplM	8	3.00E+04
<a href="#">P73320 RL3 SYN3</a>	50S ribosomal protein L3 RplC	12	2.96E+04
<a href="#">P27179 ATPA SYN3</a>	ATP synthase subunit alpha AtpA	16	2.90E+04
<a href="#">P73314 RS3 SYN3</a>	30S ribosomal protein S3 RpsC	11	2.80E+04
<a href="#">P09192 PSBD SYN3</a>	Photosystem II subunit PsbD (D2)	5	2.77E+04
<a href="#">Q55709 SECA SYN3</a>	Protein translocase subunit SecA	42	2.69E+04

The analysis was performed on Evosep ONE (Evosep Biosystems) connected to timsTOF SCP (Bruker Daltonics) using the Endurance column (4cm x150  $\mu$ m, 1.9  $\mu$ m). The identifications were quantified using IonQuant 1.10.12 with default settings for label free quantification mode. PSI-related proteins are in bold.

**Supplemental Table 3. Mass spectrometric (MS) and Western blot (WB) identification of proteins in trimeric and monomeric PSI complexes of FLAG-PSI and FLAG-PSI $\Delta$ C preparations separated in the CN gel shown in Supplemental Figure 4.**

Protein name Accession number	Mass spectrometric analysis									
	F.PSI(3)		F.PSI(1)		F.PSI $\Delta$ C(3)		F.PSI $\Delta$ C(1)'		F.PSI $\Delta$ C(1)	
	MS	WB	MS	WB	MS	WB	MS	WB	MS	WB
<b>PsaA</b> P29254	+	+	+	+	+	+	+	+	+	+
<b>PsaB</b> P29255	+	+	+	+	+	+	+	+	+	+
<b>PsaC</b> P32422	+	+	+	+	-	-	-	-	-	-
<b>PsaD</b> P19569	+	+	+	+	-	-	-	-	-	-
<b>PsbE</b> P12975	+	n.a.	+	n.a.	-	n.a.	-	n.a.	-	n.a.
<b>PsaF</b> P29256	+	+	+	+	+	+	+	+	+	+
<b>PsaI</b> Q55330	-	-	-	n.a.	-	n.a.	-	n.a.	-	n.a.
<b>PsaJ</b> Q55329	-	-	-	n.a.	-	n.a.	-	n.a.	-	n.a.
<b>PsaK1</b> P72712	+	n.a.	+	n.a.	+	n.a.	+	n.a.	+	n.a.
<b>PsaK2</b> P74564	+	n.a.	+	n.a.	+	n.a.	+	n.a.	+	n.a.
<b>PsaL</b> P37277	+	+	+	+	+	+	+	+	-	-
<b>PsaM</b> P72986	-	-	-	n.a.	-	n.a.	-	n.a.	-	n.a.

The analysis was performed on Evosep ONE (Evosep Biosystems) connected to timsTOF SCP (Bruker Daltonics) using the Endurance column (4cm x150  $\mu$ m, 1.9  $\mu$ m). n.a. means that the presence of the particular proteins was not assessed by immunodetection due to lack of appropriate antibodies. PsaI, PsaJ and PsaM were not detected by MS analysis neither, most probably due to their hydrophobic nature. Moreover, PsaI cannot be cleaved by trypsin, PsaJ theoretically gives 5 amino acid N-terminal, 9 amino acid C-terminal and 26 amino acid hydrophobic transmembrane part, all hardly detectable, and PsaM contains just a single trypsin cleavage site giving rise to hardly detectable hydrophobic 24 amino acid N-terminal and 7 amino acid C-terminal fragment.



**Supplemental Table 4. Cryo-EM single particle analysis. Summary of the data collection, refinement, and validation statistics of PSIΔC (EMDB-60522) (PDB 8ZWB).**

Data collection and processing	PSIΔC(1)
Magnification	165,000
Voltage (kV)	300
Electron exposure (e-/Å <sup>2</sup> )	34.41
Defocus range (μm)	-0.5 to -1.9
Pixel size (Å)	0.729
Initial particle images (no.)	9,991
Symmetry imposed	C1
Final particle images (no.)	333,941
<b>Map resolution (Å)</b>	
FSC threshold 0.143	1.83
<b>Refinement</b>	
Initial model used (PDB code)	5OY0
Map sharpening B factor (Å <sup>2</sup> )	-10.1
<b>Model composition</b>	
Non-hydrogen atoms	21,069
Protein residues	1,786
Ligands	147
Waters	355
<b>B factors (Å<sup>2</sup>) (min/max/mean)</b>	
Protein residues	19.04/118.34/43.20
Ligands	20.19/112.04/42.92
Waters	22.97/77.36/44.72
<b>R.m.s. deviations</b>	
Bond lengths (Å)	0.009
Bond angles (°)	1.023
<b>Validation</b>	
MolProbity score	1.14
Poor rotamers (%)	0.56
<b>Ramachandran plot</b>	
Favored (%)	98.42
Allowed (%)	1.58
Disallowed (%)	0.00

**Supplemental Table 5. Pigment and lipids composition of each PSIΔC subunit based on the cryo-EM structure.** Chls include Chl *a* (CLA) and one Chl *a'* isomer (CL0) in the reaction centre. Abbreviations: BCR - β-carotene, ECH - 5 echinenone, 5X6- zeaxanthin, LHG - 1,2-dipalmitoyl-phosphatidyl-glycerole, LMG - 1,2-distearoyl-monogalactosyl-diglycerides, and LMT - dodecyl-β-D-maltoside.

	Chlorophylls	Carotenoids			Aliphatic molecules		
	Chlorophyll <i>a</i>	BCR	ECH	5X6	LHG	LMG	LMT
<b>PsaA</b>	42	4	1	1	2	1	8
<b>PsaB</b>	43	5	1	-	1	1	9
<b>PsaF</b>	3	1	1	-	-	-	3
<b>PsaI</b>	0	1	-	-	-	-	2
<b>PsaJ</b>	2	1	1	-	-	-	3
<b>PsaK</b>	3	2	-	-	-	-	-
<b>PsaM</b>	-	-	1	-	-	-	1
<b>Total</b>	<b>93</b>	<b>14</b>	<b>5</b>	<b>1</b>	<b>3</b>	<b>2</b>	<b>26</b>

**Supplemental Table 6. List of primers used for constructing mutants used in the study (see Supplemental Figure 1).**

Primer designation	Primer name	Sequence (5' - 3')
F1	<u>psaA up1 HindIII</u>	ACAGGGAAAGCTTATACATCC
R1	<u>psaA flag R GA</u>	CTTTCGGGTGGACTAATTGTTGCGGCCGCTTTATCATCATC
F2	<u>psaA F GA</u>	ATGATGATAAAGCGGCCGCAACAATTAGTCCACCCGAAAG
R2	<u>psaA R GA</u>	ATTTGCAGATTATTGCTAGCCTAGCCAATGGAAAGACTGCG
F3	<u>psaA down F GA</u>	GCAGTCTTTCCATTGGCTAGGCTAGCAATAATCTGCAAATT
R3	<u>psaB down1 EcoRI</u>	GGCCGAATTCTTCTCTGATCC
F4	<u>psaC up 800</u>	GATACACTGGCACCAACTCCAATTCCCAGACTAGGA
R4	<u>psaC Cm up rev</u>	CGGTGGTATATCCAGTGATTTTTTCTCCATTGACTATCGGC
F5	<u>psaC up Cm fwd</u>	GGAGCCGATAGTCAATGGAGAAAAAATCACTGGATATACCACCG
R5	<u>psaC Cm dw rev</u>	ACCAGATCTATACGATCGCTTATTATCACTTATTCAGGCGTAGCAC
F6	<u>psaC dw Cm fwd</u>	GTGCTACGCCTGAATAAGTGATAATAAGCGATCGTATAGATCTGGT
R6	<u>psaC dw 400</u>	CTAATCTCCAAACGTTCTGACACCTCCTGGTTGGTCAGAC

## Methods

### Construction of *Synechocystis* mutant strains

In this work, we used the *Synechocystis* GT-P sub-strain (Tichý et al., 2016) as a wild-type strain. To express the N-terminally 1xFLAG-tagged PsaA (FLAG-PsaA) from the *psaA* promoter in *Synechocystis* (replacing the native *psaA* gene), a set of DNA constructs was prepared by the NEBuilder HiFi DNA assembly kit, each containing the gentamycin resistance cassette downstream of the *psaAB* locus (**Supplemental Figure 1A**). As the first step we replaced the whole *psaAB* operon to obtain strains expressing only the FLAG-PsaA lacking both native PsaA and PsaB proteins (*FLAG-psaA/ΔpsaB* strain). The strain expressing FLAG-PsaA instead of the original PsaA (*FLAG-psaA*) was then prepared by transforming the *FLAG-psaA/ΔpsaB* strain using the *psaB*-Gent construct and selecting for autotrophy (**Supplemental Figure 1B**). The deletion of the *psaC* gene in the *FLAG-psaA* strain was achieved by replacing most of the *psaC* gene with chloramphenicol resistance cassette (**Supplemental Figure 1B**). Segregation proceeded in low light ( $5 \mu\text{mol photons m}^{-2} \text{s}^{-1}$ ) on plates containing glucose and particular antibiotics (Komenda et al., 2008) and was confirmed by PCR using a specific set of primers (see **Supplemental Table 6**). The correct sequence of the whole modified DNA region was confirmed by DNA sequencing in all newly constructed and fully segregated strains.

### Cultivation conditions of *Synechocystis* strains

The strains were grown in 100 mL of liquid BG11 medium supplemented with 5 mM glucose using 250 mL conical flasks on a rotary shaker under  $5 \mu\text{mol photons m}^{-2} \text{s}^{-1}$  at 29 °C. For protein purification, 500 mL of cell culture in a 1-L cylinder was grown under  $5 \mu\text{mol photons m}^{-2} \text{s}^{-1}$  in BG11 medium supplemented with 5 mM glucose. The cell culture was agitated with a magnetic stirrer and bubbled with air.

### Absorption spectroscopy and pigment determination

Absorption spectra of the preparations were measured at room temperature using a UV-3000 spectrophotometer (Shimadzu, Japan) in the 25 mM MES/NaOH, pH 6.5, 10 mM  $\text{CaCl}_2$ , 10 mM  $\text{MgCl}_2$ , and 25% glycerol (thylakoid buffer) containing 0.05% n-dodecyl- $\beta$ -D-maltoside (DDM). The spectra were normalized to the 680 nm peak of Chl. Light-induced absorption changes of the oxidized primary donor of PSI RC (P700+) in the 580-780 nm range were recorded using a locally built kinetic spectrometer described in detail previously (Bína et al. 2006). Oxidized P700 was accumulated by a 3 s pulse of blue (470 nm) light corresponding to irradiance of  $\sim 2000 \mu\text{mol photons m}^{-2} \text{s}^{-1}$  delivered by a high-power LED (M470L3, Thorlabs, USA). The sample was supplied with  $\sim 20$  mM sodium ascorbate.

For routine Chl determination, pigments were extracted from cell pellets with 100% methanol and Chl concentration was determined spectroscopically (Wellburn, 1994). The amount of Chl and carotenoids per a single PSI reaction centre was determined by HPLC (Agilent 1260) using the following method: The sample was mixed with an excess of 100% methanol and the extracted pigments were separated on a reverse-phase column Zorbax Eclipse Plus C18 (4.6 x 250 mm, 5  $\mu$ m, Agilent) with 32% (v/v) methanol and 14% (v/v) acetonitrile in 0.25M pyridine (solvent A) and 20% (v/v) methanol, 20% (v/v) acetone, 60% (v/v) acetonitrile as solvent B. Pigments were eluted with a linear gradient of solvent B (60–100% (v/v) in 40 min) in solvent A followed by 100% of solvent B in solvent A for 30 min at a flow rate of 0.8 ml min<sup>-1</sup> at 40 °C. Chl-*a* and carotenoids were detected by a diode-array detector (Agilent 1260) at 450 nm, the obtained peaks were integrated, and the molar stoichiometries calculated from calibration curves that were prepared using authentic standards. Chl-*a* C13<sup>2</sup> epimer was detected by a fluorescence detector (Agilent 1260) set to 435 nm and 670 nm excitation and emission wavelengths, respectively.

#### Preparation of membranes and FLAG-specific protein purifications

Small-scale membrane fractions were prepared by breaking the cells with zirconia/silica beads using a Mini-Beadbeater (BioSpec Products, USA) according to the procedure described in (Komenda and Barber, 1995), but the cells were resuspended and broken in thylakoid buffer. Large-scale membrane preparations for the purification of proteins were carried out in thylakoid buffer containing a protease inhibitor cocktail (Roche or Sigma-Aldrich, USA) as described in (Koskela et al., 2020) with the exception that membranes were broken using Precellys Evolution (Bertin Technologies, France). Obtained membranes were solubilized with 1% DDM and FLAG-tagged proteins were isolated using the anti-FLAG M2 affinity gel (Sigma-Aldrich, USA) as described in detail in (Koskela et al., 2020).

#### Analysis of membrane protein complexes and their subunit composition

The analysis of membrane protein complexes using CN-PAGE in a 4% to 14% gradient polyacrylamide gel and the subsequent second dimension SDS-PAGE in a denaturing 12% to 20% gradient gel containing 7 M urea was performed as described in (Komenda et al., 2012). To increase denaturation of the complexes and identify Psal protein, the lanes from the native gel were excised and incubated in 25 mM Tris/HCl, pH 7.5, containing 2% SDS (w/v) at 50 °C for 20 min instead of room temperature for 30 min. The separated proteins were visualized by staining with Coomassie Brilliant Blue and detected by MS. Western blots were performed as described in (Komenda et al., 2012). The primary rabbit antibodies used in the study were specific against Psal, Psab, Psac, Psad and Psal proteins (Agrisera cat. no. AS06 172, AS10 695, AS10 939, AS09 461 and AS19 4353, respectively). The antibody against Psaf was raised against residues 50-61 of the *Synechocystis* Psaf protein.



### Mass spectrometry analysis and data interpretation for in-solution and in-gel samples

For analysis of the liquid PSIAC preparation, two  $\mu\text{l}$  of the WT and the mutant pull-downs were diluted into the 18  $\mu\text{l}$  of 50mM ammonium citrate pH 3.5 supplemented with 10% acetonitrile, 2M urea and 100mM TCEP. Subsequently, 50 ng of mucorpepsin was added to the sample and it was incubated at RT for 1hr. The desalting procedure and data-dependent mass spectrometry analysis were performed according to (Felčíková et al., 2024).

In gel digestion was performed according to Pompach et al. with minor modifications (Pompach et al., 2009). The cystamine was omitted and the in-gel reduction and alkylation was accomplished with 10mM Tris(2-carboxyethyl)phosphine and 30mM chloroacetamide at 70 °C for 10 min. After the overnight digestion, the resulting peptides were collected, the remaining gel was extracted by 5  $\mu\text{l}$  of 0.5% Trifluoroacetic acid in 50% acetonitrile. The organic fraction was pulled with the previous water fraction, the peptide extracts were diluted five times by water and loaded on Evosep tips (Evosep Biosystems). The final analysis of in-gel digests was performed on Evosep ONE (Evosep Biosystems) connected to timsTOF SCP (Bruker Daltonics) using the Endurance column (4cm x150mm, 1.9 mm) and 200 method.

In both cases, data were searched using PEAKS Studio 11 (Tran et al., 2019) (Bioinformatics Solutions Inc., Waterloo, ON, Canada). The database consisted of 1,109 *Synechocystis* protein sequences (taxonomy ID: 1142, reviewed), obtained from UniProtKB (The UniProt Consortium et al., 2023) on June 14, 2024, and 243 sequences of common contaminants. Protein digestion was set to [KR|P] for native gel digests, and as unspecific for the purified preparations, with up to 2 misscleavages and allowed peptide lengths of 5-50. Protein N-term acetylation and Met oxidation were set as variable modifications, with a maximum of 2 modifications per peptide. The tolerance for precursors and fragments was set to 12 ppm and 0.05 Da, respectively. FDR thresholds were set to 1% on both the PSM and protein level. Only proteins with 2 and more unique peptides were accepted. The proteins were quantified by PEAKS as the total area of peptide features from unique supporting peptides.

Data were deposited to the ProteomeXchange Consortium via the PRIDE partner repository with the data set identifier PXD053754.

### Cryo-EM single particle analysis:

Holey carbon grids for structural analysis were prepared using a PSIAC sample with Chl concentration of 1.5 mg/ml. The grids (Cu 300 mesh 1.2/1.3, Quantifoil) were glow discharged for 60 sec with 30 mA using a GloQube (Quorum) instrument. 3  $\mu\text{l}$  of the protein sample were pipetted onto the glow-discharged grids, blotted for 2.5 sec, and plunge frozen in liquid ethane using a Vitrobot Mark IV (Thermo Fisher Scientific) which was adjusted to a temperature of 4 °C and a relative humidity of 100%. Clipped grids were imaged using a 300 kV Titan Krios G4 microscope (Thermo Fisher Scientific) that

is equipped with a Selectris Energy filter (Slit width 10 eV) and a Falcon 4i detector. Grid screening and data collection were carried out using EPU software (v3.5.1.6034). 9,991 movies were recorded at a nominal magnification of 165,000, which corresponds to a pixel size of 0.729 Å. The total dose per micrograph was 34.41 e/Å<sup>2</sup>, and a defocus range of -0.5 to -1.9 was collected. Movies were processed using the live version of cryoSPARC v4.4.0 (Punjani et al., 2017). Motion correction, CTF estimation, blob/template picking, and 2D classification were performed. *Ab initio* reconstruction was performed in cryoSPARC to get a low-resolution reconstruction. Subsequently, an intermediate-resolution reconstruction was generated using homogeneous refinement in cryoSPARC. This map and four additional junk classes were used as references in a heterogeneous refinement job using all picked particles as input. This enriched the number of good particles. The good particles were re-extracted (unbinned, 350 px box) for a subsequent non-uniform refinement job in cryoSPARC. The particle information was then converted into a Star file using csparc2star of PyEM (UCSF pyem v0.5. Zenodo). The x-y coordinates were used to re-extract particles in RELION (Scheres, 2012). Following a local angular search in 3D refinement, a 3D classification with two classes was carried out. The class with a lower particle number (333,941) but higher resolution was considered to contain better-quality particles and was used in subsequent steps. Multiple rounds of 3D refinement, followed by CTF refinement and Bayesian polishing, were conducted. Finally, a 3D reconstruction was obtained with an overall resolution of 1.83 Å (**Supplemental Figure 5**).

#### Model building and refinement:

Model building was carried out using Coot 9.8.9 (Emsley et al., 2010). The coordinates from the PDB entry 5OY0 were used as the starting model. The PDB was rigid-body fitted into our highest resolution map at 1.83 Å using UCSF Chimera (Pettersen et al., 2004). All deviations from the starting model, such as chain deletion, correction of rotamers, rebuilding of local sections, building of water molecules, and other improvements in model quality, were carried out using Coot. The model-to-map weight was adjusted manually according to the local quality of the map. For all ligands, restraint files were generated using the Grade2 server (<http://grade.globalphasing.org>). The final model was then refined using PHENIX Real-Space-Refine (Afonine et al., 2018). The refinement protocol was optimized by variations of different weights (overall weight, Ramachandran weight). Several iterations of rebuilding, refinement, and validation were carried out using Coot, Real-space-Refine, and PHENIX (Afonine et al., 2018). The final model and its corresponding maps were validated using the PDB validation server (<https://validate-rcsb-1.wwpdb.org/>) and were subsequently deposited into the PDB databank. Structural figures were generated using UCSF ChimeraX (Pettersen et al., 2021).

## REFERENCES :

- Afonine, P. V., Poon, B. K., Read, R. J., Sobolev, O. V., Terwilliger, T. C., Urzhumtsev, A., and Adams, P. D.** (2018). Real-space refinement in *PHENIX* for cryo-EM and crystallography. *Acta Crystallogr D Struct Biol* **74**:531–544.
- Bína D, Litvín R, Vácha F, Šiffel P (2006) New multichannel kinetic spectrophotometer-fluorimeter with pulsed measuring beam for photosynthesis research. *Photosynth Res* **88**:351–356
- Emsley, P., Lohkamp, B., Scott, W. G., and Cowtan, K.** (2010). Features and development of *Coot*. *Acta Crystallogr D Biol Crystallogr* **66**:486–501.
- Felčíková, K., Hovan, A., Polák, M., Loginov, D. S., Holotová, V., Díaz, C., Kožár, T., Lee, O., Varhač, R., Novák, P., et al.** (2024). Design of ASLOV2 domain as a carrier of light-induced dissociable FMN photosensitizer. *Protein Science* **33**:e4921.
- Komenda, J., and Barber, J.** (1995). Comparison of psbO and psbH deletion mutants of *Synechocystis* PCC 6803 indicates that degradation of D1 protein is regulated by the QB site and dependent on protein synthesis. *Biochemistry* **34**:9625–9631.
- Komenda, J., Nickelsen, J., Tichý, M., Prášil, O., Eichacker, L. A., and Nixon, P. J.** (2008). The Cyanobacterial Homologue of HCF136/YCF48 Is a Component of an Early Photosystem II Assembly Complex and Is Important for Both the Efficient Assembly and Repair of Photosystem II in *Synechocystis* sp. PCC 6803. *Journal of Biological Chemistry* **283**:22390–22399.
- Komenda, J., Knoppová, J., Kopečná, J., Sobotka, R., Halada, P., Yu, J., Nickelsen, J., Boehm, M., and Nixon, P. J.** (2012). The Psb27 Assembly Factor Binds to the CP43 Complex of Photosystem II in the Cyanobacterium *Synechocystis* sp. PCC 6803. *Plant Physiology* **158**:476–486.
- Koskela, M., Skotnicová, P., Kiss, É., and Sobotka, R.** (2020). Purification of Protein-complexes from the Cyanobacterium *Synechocystis* sp. PCC 6803 Using FLAG-affinity Chromatography. *BIO-PROTOCOL* **10**.
- Pettersen, E. F., Goddard, T. D., Huang, C. C., Couch, G. S., Greenblatt, D. M., Meng, E. C., and Ferrin, T. E.** (2004). UCSF Chimera—A visualization system for exploratory research and analysis. *J Comput Chem* **25**:1605–1612.
- Pettersen, E. F., Goddard, T. D., Huang, C. C., Meng, E. C., Couch, G. S., Croll, T. I., Morris, J. H., and Ferrin, T. E.** (2021). UCSF ChimeraX: Structure visualization for researchers, educators, and developers. *Protein Sci* **30**:70–82.
- Pompach, P., Man, P., Kavan, D., Hofbauerová, K., Kumar, V., Bezouška, K., Havlíček, V., and Novák, P.** (2009). Modified electrophoretic and digestion conditions allow a simplified mass spectrometric evaluation of disulfide bonds. *J. Mass Spectrom.* **44**:1571–1578.
- Punjani, A., Rubinstein, J. L., Fleet, D. J., and Brubaker, M. A.** (2017). cryoSPARC: algorithms for rapid unsupervised cryo-EM structure determination. *Nat Methods* **14**:290–296.

- Scheres, S. H. W.** (2012). RELION: Implementation of a Bayesian approach to cryo-EM structure determination. *Journal of Structural Biology* **180**:519–530.
- The UniProt Consortium, Bateman, A., Martin, M.-J., Orchard, S., Magrane, M., Ahmad, S., Alpi, E., Bowler-Barnett, E. H., Britto, R., Bye-A-Jee, H., et al.** (2023). UniProt: the Universal Protein Knowledgebase in 2023. *Nucleic Acids Research* **51**:D523–D531.
- Tichý, M., Bečková, M., Kopečná, J., Noda, J., Sobotka, R., and Komenda, J.** (2016). Strain of *Synechocystis* PCC 6803 with Aberrant Assembly of Photosystem II Contains Tandem Duplication of a Large Chromosomal Region. *Front. Plant Sci.* **7**.
- Tran, N. H., Qiao, R., Xin, L., Chen, X., Liu, C., Zhang, X., Shan, B., Ghodsi, A., and Li, M.** (2019). Deep learning enables de novo peptide sequencing from data-independent-acquisition mass spectrometry. *Nat Methods* **16**:63–66.
- Wellburn, A. R.** (1994). The Spectral Determination of Chlorophylls a and b, as well as Total Carotenoids, Using Various Solvents with Spectrophotometers of Different Resolution. *Journal of Plant Physiology* **144**:307–313.